J Mater Sci (2011) 46:1184–1189
DOI 10.1007/s10853-010-4891-8

Luminescence properties of monodispersed spherical $BaWO_4:Eu^{3+}$ microphosphors for white light-emitting diodes

Jinsheng Liao · Bao Qiu · He-Rui Wen · Yong Li · Ruijin Hong · Hangying You

Received: 9 May 2010 / Accepted: 31 August 2010 / Published online: 14 September 2010

Abstract Monodispersed spheres (1–4 μm in diameter) of $BaWO_4:Eu^{3+}$ (hereafter BWO:Eu) red-phosphor exhibiting intense emission at 615 nm were synthesized via a mild hydrothermal method. X-ray diffraction, scanning electron microscope, photoluminescence excitation and emission spectra, and decay curve were used to characterize the properties of BWO:Eu phosphors. An intense red emission was obtained by exciting either into the $^5L_6$ state with 394 nm or the $^5D_2$ state with 465 nm, that correspond to two popular emission lines from near-UV and blue LED chips, respectively. The values of $\Omega_{2,4}$ experimental intensity parameters (13.8×10^{-20} and 8.2×10^{-20} cm^2) are determined. The high-emission quantum efficiency of the BWO:Eu phosphor suggests this material could be promising red phosphors for generating white light in phosphor-converted white light-emitting diodes.

Introduction

Recently, white light-emitting diodes (WLEDs) have received much attention because of high luminous efficiency, energy-saving, long life, and environmental protection. Therefore, they called the next-generation solid-state light and they can replace conventional incandescent and fluorescent lamps [1]. There are several approaches to make white LEDs. One approach is a blue LED chip (GaN) coated by yellow phosphor (YAG:Ce) to produce white light [2, 3]. Another approach is a near-UV LED chip (InGaN) with a combination of red/green/blue tricolor phosphors [4]. However, The commercial WLED for GaN-based YAG:Ce phosphor has low color-rendering index and high color temperature due to the spectral scarcity in red region. The key to improve the color-rendering index is to enrich the red emission of WLEDs. Thus, there is a great need to develop a novel red-emitting phosphor. However, it is an attractive and challenging research task to explore a novel efficient red-emitting phosphor applied in near-UV LED.

The alkaline-earth metal tungstates MWO_4 ($M = Ca^{2+}$, Sr^{2+}, Ba^{2+}) were reported to be efficient luminescent hosts for rare earth elements [5–9]. $BaWO_4$ is an important member of alkaline-earth metal tungstate families, which has been generally considered as scheelite-structure compounds. Many methodologies including flux method [10], conventional solid-state reactions [11], precipitation technique [12], microwave hydrothermal method [13], and reversed micelle template method [14] have been extensively investigated to prepare pure $BaWO_4$, but still face issues in efficient control over the morphology and particle size that are crucial for high luminescence performance. Wet chemistry via hydrothermal processes is advantageous for homogeneous nucleation of microcrystals with defined morphologies. However, to the best of our knowledge, there has been no report on the research of BWO:Eu microcrystal for potential application as a red phosphor in WLEDs.

In this article, we prepared monodispersed spheres for BWO:Eu phosphor with different Eu^{3+} content by a hydrothermal method. The substitution of Eu^{3+} at Ba^{2+} site (S_4) was determined based on excitation, emission spectra, the luminescence decay curve, and crystal structure. The Judd–Oflet (JO) intensity of Eu^{3+} in BWO:Eu phosphor was investigated.

J. Liao (✉) · B. Qiu · H.-R. Wen · Y. Li · R. Hong · H. You
School of Material and Chemistry Engineering,
Jiangxi University of Science and Technology,
Ganzhou, Jiangxi 341000, China
e-mail: jsliao1209@126.com

Experimental

Preparation

The initial chemicals of Eu_2O_3 (with purity of 99.99%), $Ba(NO_3)_2$, $Na_2WO_4{\cdot}2H_2O$, NaOH, HNO_3, and citric acid (all with purity analytical reagent) were purchased from shanghai chemical Industrial Co, and were used without further purification. All BWO:Eu samples were prepared by a facile hydrothermal process. First, Eu_2O_3 was dissolved in dilute nitric acid under heating, resulting in the formation of a colorless stock solution of $Eu(NO_3)_3$ with 0.05 mol/L. In a typical synthesis, 15-mL $Eu(NO_3)_3$ solution was extracted from the above solution. Then 0.4573-g $Ba(NO_3)_2$ and 0.2627-g citric acid as chelating agent for the metal ions were added into the $Eu(NO_3)_3$ solution while stirring. The molar ratio of citric acid to metal ions was 2:1. Meanwhile 0.8246-g $Na_2WO_4{\cdot}2H_2O$ was slowly added to the mixed solution until a little white precipitate formed. 10 wt% of NaOH solution was introduced dropwise to the vigorously stirring to pH 9 to form a little white precipitate. After additional agitation for 2 h, the above solution of white precipitate contained was transferred into a 50-mL autoclave, sealed and heated to 180 °C for 12 h. It was then cooled to room temperature naturally. The products were collected by centrifugation, washed with distilled water and ethanol for three times, dried in air at 100 °C for 4 h. The other phosphors with different Eu^{3+}-doped concentrations were synthesized by the same procedure with corresponding starting materials.

Characterization

The crystalline phase of samples was analyzed by an X-ray diffractometer (PANalytical X'Pert Pro) using Cu $K\alpha_1$ radiation ($\lambda = 0.154187$ nm). The morphology of the samples was inspected using a scanning electronic microscope (SEM Philips XL30). The photoluminescence (excitation and emission) spectra and the luminescence decay were recorded on an Edinburgh Instruments FLS920 spectrofluorimeter equipped with both continuous (450 W) xenon and pulsed xenon (microsecond) lamps. The line intensities of the excitation spectra were calibrated for the wavelength dependence of the instrument response including the intensity of the xenon lamp, the transmission efficiency of monochromators, and the quantum efficiency of detector. The line intensities of emission spectra were calibrated for the wavelength dependence of the instrument response by the quantum efficiency of detector and the transmission efficiency of monochromator. The line positions of the measured spectra were calibrated according to standard mercury lamp. All measurements were performed at room temperature.

Results and discussion

Powder XRD and SEM studies

The crystallinity and phase purity of the as-prepared samples were examined with XRD. Figure 1 presents XRD patterns of the BWO:Eu samples with different Eu^{3+}-doped concentrations. From Fig. 1, it can be seen that all diffraction peaks matched well the standard data of scheelite phase $BaWO_4$ (JCPDS card NO: 72-0746), and that no traces of additional peaks from other phases were observed. Therefore, every as-prepared sample was a single-phase $BaWO_4$ with the scheelite structure. It is shown in Fig. 1 that the peaks of the XRD patterns become weak and slightly broad with increasing Eu^{3+} concentration. It is indicated that the crystal size is gradually reduced with increasing Eu^{3+} concentration. SEM images (Fig. 2) for BWO:Eu phosphors with different Eu^{3+} concentration (1, 5, 10, 12, 15, and 17 at.%) showed the morphologies were spherical and the average sizes of particles are 4.5, 4.2, 2.8, 2.7, 2.2, and 0.8 μm in diameter without aggregating, respectively. The average sizes of BWO:Eu phosphors gradually decrease with increasing Eu^{3+} concentration. The results of SEM agree with those of XRD.

To validate the actual Eu^{3+} concentration in as-prepared BWO:Eu phosphors, the chemical analyses of the as-prepared samples were performed by a Shimadzu 8705QH_2 electron probe X-ray microanalyser (EPMA) and an Oxford Instruments INCA energy dispersive spectrometer (EDS). In the EDS spectra, the signals of europium (Eu), barium (Ba), tungsten (W), and oxygen (O) suggest the presence of corresponding element for all the samples (see Fig. 2). The approximate surface composition extracted from the EDS analysis gives a Eu/Ba/W atomic ratio of

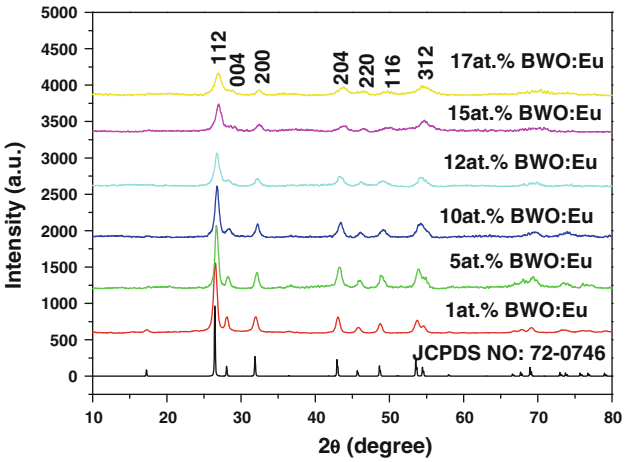

Fig. 1 (Color online) XRD patterns for BWO:Eu sample with different Eu^{3+}-doped concentrations. The standard data for scheelite-type BWO (JCPDS No.72-0746) is also presented in the figure

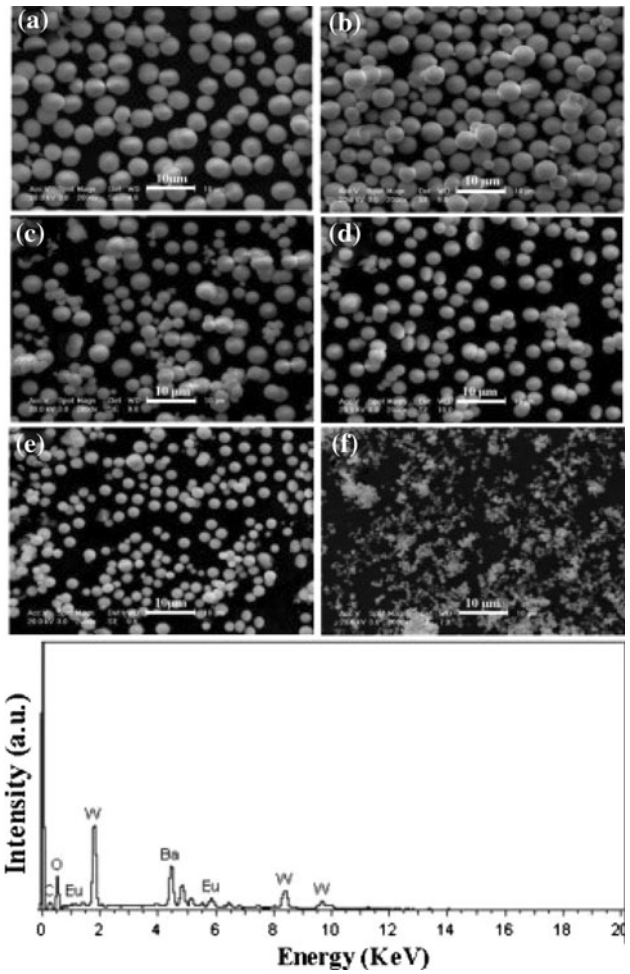

Fig. 2 SEM images of the BWO:Eu phosphors with different Eu^{3+}-doped concentrations. **a** 1 at.%, **b** 5 at.%, **c** 10 at.%, **d** 12 at.%, e 15 at.%, f 17 at.%, and EDS spectrum for the BWO:Eu phosphor

0.145:0.855:1, which is very close to that of the starting material (15 at.% BWO:Eu). Moreover, the analytical results of BWO:Eu phosphors with different Eu^{3+}-doped concentrations are also close to those of the starting material. Therefore, the doping concentrations of Eu^{3+} in the starting materials are adopted as the actual concentration of Eu^{3+}-doped $BaWO_4$ phosphors. The signal of sodium (Na) was not detected in all the samples. Thus, the charge compensation mechanism of $BaWO_4$:Eu^{3+} phosphors may be that three Ba^{2+} ions are replaced by two Eu^{3+} ions and one vacancy, $3Ba^{2+} = 2Eu^{3+}+V_{Ba}$ (where V_{Ba} is a Ba site vacancy).

Photoluminescence studies

Figure 3 shows the excitation spectrum of 15 at.% BWO:Eu phosphor by monitoring the emission at 615 nm which corresponds to the $^5D_0 \rightarrow {}^7F_2$ transition. The broad band centered at 261 nm is due to the combination of

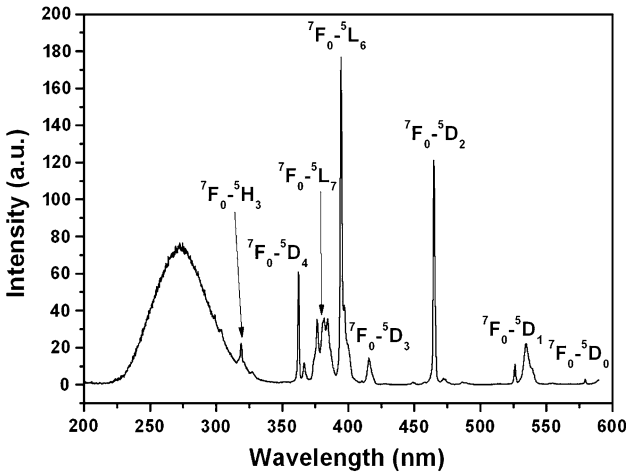

Fig. 3 Excitation spectrum of 15 at.% BWO:Eu sample, monitoring the Eu^{3+} emission at 615 nm

charge transfer transitions from O-Eu^{3+} and O–W group [15]. In addition, the sharp f–f transitions of Eu^{3+} ($^7F_0 \rightarrow {}^5D_{0.1.2.3.4}$, $^5L_{6.7}$, $^5H_3$) [15] are clearly marked in Fig. 3. Among these excitation transitions, $^7F_0 \rightarrow {}^5L_6$ (394 nm) and $^7F_0 \rightarrow {}^5D_2$ (464 nm) lines [15] are the most intense ones, which are located at the emission wavelength of near-UV (380–410 nm) and blue (~460 nm) LEDs. Therefore, BWO:Eu phosphors can be effectively excited by radiations of wavelength in near-UV and blue regions, and then emits bright red light.

Figure 4 displays the emission spectrum of 15 at.% BWO:Eu phosphor under the excitation wavelengths of irradiation 394 and 465 nm at room temperature. The emission peaks are similar for different excitation wavelength.

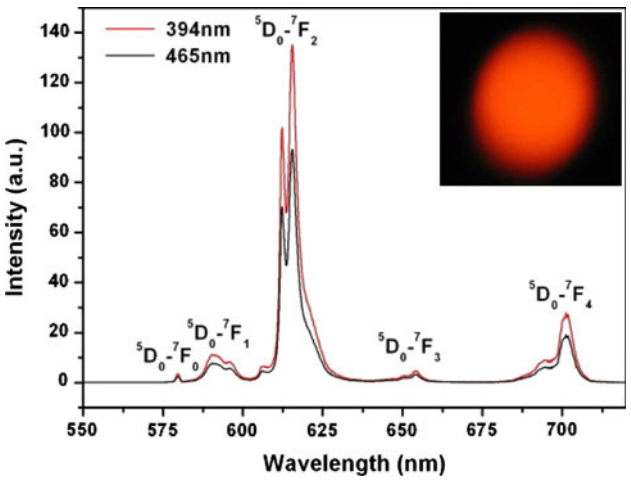

Fig. 4 (Color online) Emission spectrum of 15 at.% BWO:Eu sample under 394 and 465 nm excitation. The *insets* are color photos of BWO:Eu. Phosphor was excited with a Xenon lamp at 394 nm. To eliminate the influence of excitation, a 495-nm long pass glass filter was used to take this photo

However, it can be seen from Fig. 4 that the red emission intensity excited at near-UV radiation (394 nm) is greater than that of excited at blue region 465 nm. The forced electric-dipole transition of Eu^{3+} ions ($^5D_0 \rightarrow {}^7F_2$) gives a set of red emission peaks at 606, 612, and 615 nm. It is worth mentioning that the most intensive emission peak at 615 nm is narrow with a full width at half-maximum (fwhm) less than 5 nm, indicating that Eu^{3+} ion may be incorporated in the BWO matrix. The $^5D_0 \rightarrow {}^7F_1$ (591 nm) transition is the parity-allowed magnetic dipole (MD) transition, which is insensitive to the chemical surroundings of the luminescent center and its symmetry. For instance, the $^5D_0 \rightarrow {}^7F_2$ forced electronic-dipole (ED) transition becomes the strongest one when Eu^{3+} ions are situated at low symmetries with no inversion center, while the $^5D_0 \rightarrow {}^7F_1$ MD transition is dominant when they are situated at high symmetries with inversion center. Therefore, the intensity ratio (R/O) of the transitions $^5D_0 \rightarrow {}^7F_2$ to $^5D_0 \rightarrow {}^7F_1$ is a good probe for the symmetry of Eu^{3+} site. The red emission intensity (R) of $^5D_0 \rightarrow {}^7F_2$ transition is much higher than the orange one (O) of $^5D_0 \rightarrow {}^7F_1$, and the R/O value calculated for 15 at.% BWO:Eu phosphor is 6.85. In addition, $BaWO_4$ crystallizes into a scheelite-like tetragonal structure with space group C_{4h}, in which Ba^{2+} is coordinated with eight oxygen atoms and has a S_4 point symmetry with no inversion center. These considerations make us to assume that Eu^{3+} may be doped into the Ba^{2+} sites of the samples, in agreement with the ionic radii difference because the ionic radii of 1.07 Å for Eu^{3+} is smaller than that of 1.42 Å for Ba^{2+}, but much larger than that of 0.42 Å for W^{6+} in 4-fold coordination. The $^5D_0 \rightarrow {}^7F_0$ transition shows only one peak for BWO:Eu phosphor (Fig. 4), suggesting the existence of one site symmetry for the Eu^{3+} ion chemical environment. The results are also in agreement with the single exponential behavior in the luminescence decay curve of the emitting $^5D_0$ level in aftermentioned discussion.

By changing the content of Eu^{3+} ion in BWO phosphor, the optimum compositions were determined by the highest emission intensity. In all emission spectra, the peak positions and peak width did not change with the change of Eu^{3+} content. It implies that the Eu^{3+} ions can be effectively incorporated BWO matrix with increasing Eu^{3+} content. But for the emission intensities, they changed with the Eu^{3+} content. Figure 5 shows the dependence of the red emission intensity of Eu^{3+} ($^5D_0 \rightarrow {}^7F_2$) on Eu^{3+} content. From Fig. 5, it is evidently seen that the emission intensity increases with increasing Eu^{3+} content till reaching a maximum value at 15 at.%, and then decreases with increasing its content over 15 at.% due to the concentration quenching effect.

Furthermore, to better understand the effect of chemical environment on the luminescence properties of Eu^{3+}, the JO intensity parameters $\Omega_{2,4}$ of Eu^{3+} in BWO phosphor can be

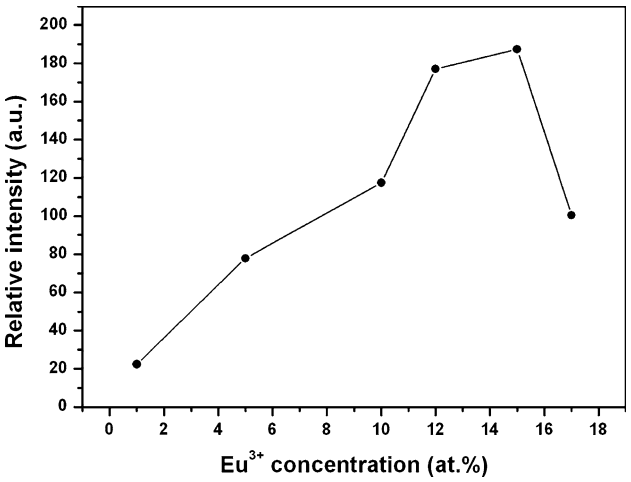

Fig. 5 The photoluminescence emission intensity (integrated intensity of $^5D_0 \rightarrow {}^7F_2$) of Eu^{3+} ions as a function its doping concentration in BWO host

calculated directly using the method proposed by Krupke [16]. This method makes use of the fact that the intensities of the $^5D_0 \rightarrow {}^7F_2$, and $^5D_0 \rightarrow {}^7F_4$ transitions are solely dependent on the Ω_2 and Ω_4 parameters, respectively. Because the radiative transition rate is proportional to the integrated intensity of the transition band in the emission spectrum (i.e., $A_{(J\rightarrow J')} \propto \int \lambda I_{J(\lambda)}\, d\lambda$), the radiative transition rate of $^5D_0 \rightarrow {}^7F_J$ ($J = 0$, 2–4) can be estimated according to the ratio of the integrated intensity of $^5D_0 \rightarrow {}^7F_1$ to these transitions. The calculated radiative transition rate of $^5D_0 \rightarrow {}^7F_1$ is used as a reference to scale the absolute ED transition rates of $^5D_0 \rightarrow {}^7F_J$ ($J = 2$, 4) by [16]

$$A_{\mathrm{MD}}(J \rightarrow J') = \frac{64\pi^4 e^2 n^3}{3h(2J+1)\overline{\lambda}^3}\left(\frac{e\hbar}{2mc}\right)^2 |\langle \Phi J \| J + 2S \| \Phi' J' \rangle|^2 \quad (1)$$

where n is the index of refraction for the phosphors, for BWO crystal, an average index of refractive equal to 1.84 is used [17]; $\overline{\lambda}$ is the mean wavelength of the emission band; $|\langle \Phi J \| J + 2S \| \Phi' J' \rangle|$ are the reduced matrix elements (RMEs) of the MD operator [18]. Once the ED radiative transition rates of $^5D_0 \rightarrow {}^7F_J$ ($J = 2$, 4) are determined, the JO intensity parameters $\Omega_{2,4}$ can be calculated using the following formula [16]

$$A_{\mathrm{ED}}(J \rightarrow J') = \frac{64\pi^4 e^2}{3h(2J+1)\overline{\lambda}^3}\frac{n(n^2+2)^2}{9}\sum_{t=2,4,6}\Omega_t \left|\left\langle \Phi J \left\| U^{(t)} \right\| \Phi' J' \right\rangle\right|^2 \quad (2)$$

The square reduced matrix elements $\left|\left\langle \Phi J \left\| U^{(t)} \right\| \Phi' J' \right\rangle\right|^2$ are obtained from those values of Eu^{3+}:LaF_3 [18] because they are insensitive to the host. According to the emission spectra, the JO intensity parameters $\Omega_{2,4}$ were determined

Table 1 Luminescence parameters for the BWO:Eu phosphor and Eu-doped tungstates at room temperature

Phosphors	A_{rad} (s^{-1})	A_{nrad} (s^{-1})	A_{tot} (s^{-1})	Ω_2 ($10^{-20}cm^2$)	Ω_4 ($10^{-20}cm^2$)	τ_l (ms)	η (%)	References
BWO:Eu	1186	377	1563	13.8	8.2	0.64	76	[a]
$CaWO_4$:Eu	950	82	1032	/	/	0.97	92	[5]
$La_2(WO_4)_3$:Eu	1024	481	1505	25.8	13.1	0.66	68	[15]

[a] The date from this study

to be 13.8, 8.2 for Eu^{3+} in units of 10^{-20} cm^2. The Ω_6 intensity parameter was not included in this calculation because the transition of $^5D_0 \rightarrow {}^7F_6$ proved to be too weak to observe in our experimental setup. It can be inferred from the known minimum detectable power of the system that Ω_6 must be less than 2.5×10^{-21} cm^2. Table 1 compares the JO parameters of Eu^{3+} in different tungstate hosts. The very small Ω_6 of BWO:Eu, similar to that of $La_2(WO_4)_3$, is presumably ascribed to the relatively small fifth- and seventh-order crystal field (CF) components [16, 19]. The variation of Ω_2, reflected by the hypersensitivity of the $^5D_0 \rightarrow {}^7F_2$ transition, can be related to a variation in the covalency of the Eu–O bond as well as in the structural environment around Eu^{3+} ions [20]. The values of Ω_2 for Eu^{3+} in $La_2(WO_4)_3$:Eu matrix are nearly twice as that of BWO:Eu microcrystal, since Eu^{3+} in $La_2(WO_4)_3$:Eu possesses a low symmetry of C_{nv} site, while Eu^{3+} in BWO:Eu microcrystal possesses a high symmetry of S_4 site. However, the value of Ω_2 for Eu^{3+} in BWO:Eu microcrystal is greater than that of the $[Eu(H_2O)_6](ClO_4)_3$ complex in the O_h symmetry ($\Omega_2 = 1.1 \times 10^{-20}$ cm^2) [21]. Therefore, the relatively large value of Ω_2 for Eu^{3+} in BWO:Eu microcrystal may suggest an enhanced covalency or shorter bond length between Eu^{3+} and oxide anions and a relatively low site symmetry of Eu^{3+}.

Further, the emission quantum efficiency (η) of the $^5D_0$ excited state of Eu^{3+} ions in BWO phosphor is determined on the basis of the emission spectra and lifetime of the $^5D_0$ emitting level. The luminescence lifetime (τ_l) is recorded at room temperature for the $^5D_0$ excited state of the Eu^{3+} ions in BWO:Eu phosphor. The representative luminescence decay curve of 15 at.% BWO:Eu phosphor is shown in Fig. 6. The decay curve for $^5D_0 \rightarrow {}^7F_2$ (615 nm) of Eu^{3+} ions can be well fitted into a single-exponential function as $I = A\exp(-t/\tau)$ (τ and A are the luminescence lifetime and the fitting parameters), and fitting results are shown in Fig. 6. The lifetime for $^5D_0$ energy level of Eu^{3+} ions is about 0.64 ms. The lifetime of 15 at.% BWO:Eu phosphor is longer than that of 0.41 ms reported for $ZnWO_4$:Eu nanocrystals [22], but a slightly longer than that of 0.54 ms for $BaMoO_4$:Eu materials [23]. The nonradiative (A_{nrad}), radiative (A_{rad}) rates and the emission quantum efficiency of the emitting $^5D_0$ excited state (η) are related through the following equation [24]:

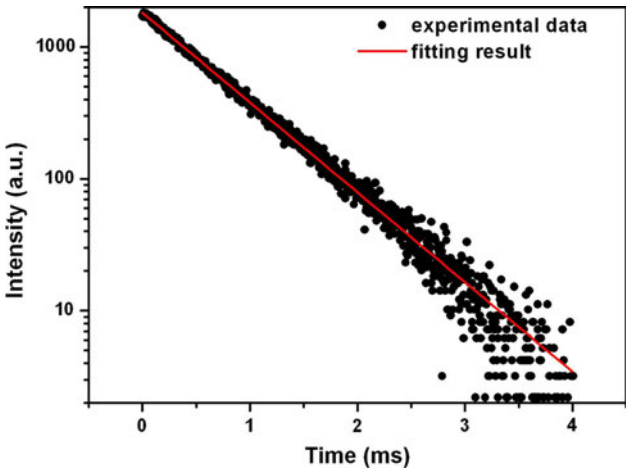

Fig. 6 (Color online) Luminescence decay of $^5D_0$ state of 15 at.% BWO:Eu (excitation wavelength 394 nm, monitoring the Eu^{3+} emission at 615 nm)

$$A_{tot} = \frac{1}{\tau_l} = A_{rad} + A_{nrad} \quad (3)$$

$$\eta = \frac{A_{rad}}{A_{rad} + A_{nrad}} \quad (4)$$

where the A_{rad} rate obtained by summing over the radiative rates A_{0J} for each $^5D_0 \rightarrow {}^7F_J$ transition is given by $A_{rad} = \sum_J A_{0J} = A_{MD} + A_{ED}$.

The luminescence quantum efficiency can be calculated from the luminescence lifetime, radiative rate. The luminescence parameters were shown in Table 1. From Table 1, the luminescent quantum efficiency of 15 at.% BWO:Eu (76%) is higher than 68% of 5 at.% $La_2(WO_4)_3$:Eu [15] prepared by Pechini method, but still lower than 92% of 4.9 at.% $CaWO_4$:Eu nanocrystal fabricated by hydrothermal process [5] and nearly 100% of commercial phosphor for Y_2O_3:Eu [25]. The high quantum efficiency suggests that BWO:Eu microcrystal can be a promising red phosphor for application in LEDs.

Conclusions

In summary, the monodispersed and spherical BWO:Eu microphosphors were synthesized by a mild hydrothermal

method at 180 °C for 12 h. The presence of only one peak assigned to the $^5D_0 \rightarrow {}^7F_0$ transition and a single-exponential fit from the luminescence decay curve of the emitting $^5D_0$ level, indicate the existence of only one symmetry site around the Eu^{3+} ion in this system. The emission spectra show strong red emission at 615 nm corresponding to the $^5D_0 \rightarrow {}^7F_2$ transition of BWO:Eu phosphors under near-UV excitation (394 nm). The optimum concentration for Eu^{3+} was determined to be about 15 at.% in BWO:Eu phosphors. Therefore, the high emission intensity, high quantum efficiency and easy preparation of this system make them potential application as red emitting phosphor in LEDs.

Acknowledgements This work has been financially supported by the Science Program of the Education Office, Jiangxi Province (No. GJJ10472) and Ganzhou City public services platform for technical innovation of nonferrous metal.

References

1. Hirosaki N, Xie RJ, Kimoto K (2005) Appl Phys Lett 86:211905
2. Nakamura S, Mukai T, Sench M (1994) Appl Phys Lett 64:1687
3. Sakuma K, Omichi K, Kimura N, Ohashi M (2004) Opt Lett 29:2001
4. Sheu JK, Chang SJ, Kuo CH, Su YK, Wu LW, Lin YC, Lai WC, Tsai JM, Chi GC, Wu RK (2003) IEEE Photon Technol Lett 15:18
5. Su YG, Li LP, Li GS (2008) Chem Mater 20:6060
6. Lei F, Yan B (2008) J Solid State Chem 181:855
7. Grobelna B, Lipowska B, Kłonkowski AM (2006) J Alloys Compd 419:191
8. Liao JS, Qiu B, Wen HR, Chen JL, You WX, Liu LB (2009) J Alloys Compd 487:758
9. Tyagi M, Sangeeta D, Sabharwal SC (2008) J Lumin 128:1528
10. Roy BN, Roy MR (1981) Cryst Res Technol 16:1267
11. Nishigaki S, Yano S, Kato H, Nonomura T (1988) J Am Ceram Soc 71:C11
12. Wang X, Xu H, Wang H, Yan H (2005) J Cryst Growth 284:254
13. Cavalcante LS, Sczancoski JC, Espinosa JWM, Varela JA, Pizani PS, Longo E (2009) J Alloys Compd 474:195
14. Shi HT, Qi LM, Ma JM, Cheng HM (2003) J Am Chem Soc 125:3450
15. Kodaira CA, Brito HF, Felinto MCFC (2003) J Solid State Chem 171:401
16. Krupke WF (1966) Phys Rev 145:325
17. Bakhshieva GF, Morozov AM (1977) Sov J Opt Technol 44:542
18. Carnall WT, Crosswhite H, Crosswhite HM (1977) Energy structure and transition probabilities of the trivalent lanthanides in LaF_3. Argonne National Laboratory Report, Argonne
19. Judd BR (1962) Phys Rev 127:750
20. Tseng YH, Chiou BS, Peng CC, Ozawa L (1998) Thin Solid Films 330:173
21. Teotonio EES, Espinola JGP, Brito HF, Malta OL, Oliveira SF, de Faria DLA, Izumi CMS (2002) Polyhedron 21:1837
22. Dai LQ, Song HW, Bai X, Pan GH, Lu SZ, Wang T, Ren XG, Zhao HF (2007) J Phys Chem C 111:7586
23. Rosa ILV, Marques APA, Tanaka MTS, Motta FV, Verela JA, Leite ER, Longo E (2009) J Fluoresc 19:495
24. Malta OL, Couto dos Santos MA, Thompson LC, Ito NK (1996) J Lumin 69:77
25. Blasse G, Crabmaie BC (1994) Luminescence materials. Springer, New York